The Pennsylvania State University

The Graduate School

Department of Mechanical and Nuclear Engineering

DECOMPOSITION AND IGNITION OF HAN-BASED MONOPROPELLANTS BY ELECTROLYSIS

A Thesis in

Mechanical Engineering

by

Prashant Khare

Submitted in Partial Fulfillment

of the Requirements

for the Degree of

Master of Science

May 2009

The thesis of Prashant Khare was reviewed and approved* by the following:

Vigor Yang
John L. and Genevieve H. McCain Chair in Engineering
Thesis Advisor

Stefan Thynell
Professor of Mechanical Engineering

Karen A. Thole
Professor of Mechanical Engineering
Head of the Department of Mechanical and Nuclear Engineering

*Signatures are on file in the Graduate School.

Abstract

In this research, electrolytically-induced HAN ignition has been studied. The purpose of the present study is to identify the various parameters and mechanisms dictating the electrolytic ignition of HAN-based monopropellants. Electrochemical mechanisms are established and incorporated into an existing chemical kinetics scheme. The ignition of HAN-water solution by electrolysis has been treated numerically using a constant pressure, homogeneous reactor model. A stiff ODE solver was used in the analysis to handle the highly stiff species conservation and the energy equations. The analysis focuses on the temporal evolution of temperature and condensed and gas phase species. Parametric studies were conducted to investigate the effect of electric current, voltage, volume, initial temperature, and HAN concentration on the ignition time delay. The ignition time delay is found to decrease with increase in current, temperature, and HAN concentration and increase with volume.

Table of Contents

List of Figures

List of Tables

Acknowledgements

I am most grateful and indebted to my thesis advisor, Professor Vigor Yang for giving me an opportunity to work under him and kindly providing guidance throughout the development of the study. He has been the source of inspiration and his support, encouragement, and comments have been of greatest help at all times.

I take this opportunity to express my love and sincere thanks to my parents and my sister for their endless love and support. They taught me the value of hard work and provided me with enormous support throughout my life.

1 Introduction

Hydroxylammonium nitrate (HAN) with the chemical formula $[NH_3OH]^+[NO_3]^-$ and HAN-based monopropellants have their genesis in the development of liquid gun propellants (1), (2). HAN-based propellants are also being considered as a replacement for hydrazine in space propulsion systems. HAN-based propellants have been considered promising monopropellants for space propulsion applications, because of their high-energy, high-density (Table 1), safe and environmentally benign characteristics (3), (4). It is quite evident from Table 2 that the rocket performance parameter, density I_{sp}, is considerably more for HAN as compared with hydrazine. Moreover HAN-based monopropellants also have a low glass-transition point, are relatively stable, have low toxicity and are easy to demilitarize and dispose (5).

HAN is oxygen rich, and is commonly referred to as the oxidizer, the other compound being fuel rich and referred to as the fuel. The physical and thermo-chemical properties of HAN are listed in Table 3. Toxicity is measured in LD_{50}, an acronym of Lethal Dose50. It is a standard measure for expressing and comparing the toxicity of chemicals. LD_{50} is defined as the dose that kills half (50%) of the animals tested. The animals are usually rats or mice, although rabbits, guinea pigs, hamsters, and so on are sometimes used. Most common units are milligram of chemical per kilogram of test animal (mg/kg). The state-of-the-art (SOA) monopropellant, hydrazine has an LD_{50} value of 59 mice (6) which clearly shows that it is much more toxic than HAN-based propellants having a much higher LD_{50} value of 325 rats. The variation of density and specific heat of HAN-water solutions with concentration is shown in Table 4 the concentration being expressed in units of molarity, M, defined as the number of moles of solute dissolved in 1*l* of the solution.

Qualitatively, the ground operation costs of a HAN-based monopropellant system can be more closely equated to a stored gas system than a hydrazine monopropellant system. HAN-based monopropellants pose only a very limited hazard when compared to hydrazine because the HAN-based formulations are nonflammable and non explosive at atmospheric pressure, are non-carcinogenic, and have a vapor head composed only of water (2).

Table 1. Comparison of physical and thermo-physical properties of HAN and Hydrazine

Properties	**HAN (100%)**	**N_2H_4 (100%)**
Melting point (K)	321	275.16 (7)
Density (kg/m^3)	1830	1003.7 (7)
Heat of formation (kcal/mol)	-79.68	12.054 (7)
Toxicity	325 mice	59 rats (6)

Table 2. Comparison of performance parameters of HAN-based monopropellants and Hydrazine

Propellant	**Vacuum I_{sp} @ 1atm (s)** (8)	**Density (kg/m^3)**	**Density I_{sp} (kg/m^3-s)**
Hydrazine	227.35	1003.7	$228.19 * 10^3$
HAN (100%)	217.85	1830.0	$398.67 * 10^3$
13 M HAN-water solution	168.35	1537.0	$258.75 * 10^3$
10.7 M HAN-water solution	135.5	1449.0	$196.34 * 10^3$

Personnel hazards are limited to skin absorption. Coveralls, gloves and face shields are sufficient for protection. By using HAN-based monopropellants, ground operations required to

handle the SOA monopropellant (hydrazine) can be modified in a number of ways. First, because there are no vapor hazards associated with HAN based monopropellants the need for Self-Contained Atmospheric Protective Ensemble (SCAPE) (9) and the associated training should be eliminated, along with simplification of health monitoring procedures for ground operations crews. This reduces the support required by environmental health and safety personnel. Secondly, because of the absence of vapor hazard and since the propellant is non-flammable at atmospheric pressure, fueling procedures can be simplified by reducing and/or eliminating fire personnel during fueling (2). Other savings can be realized by the elimination of access restrictions during fueling and the simplification of the disposal of rinse water and propellant.

Table 3. Properties of HAN

Freezing Point (K) 75/25 HAN-water solution	243 (10)
Melting Point (K) (Pure HAN)	321 (11)
Density (kg/m^3) @ 298K	1830 (12)
Enthalpy of formation (*l*) (kcal/mol)	-79.68 (13)
Theoretical Vacuum I_{sp} (s) @ 100 psi / 50:1	262.6 (LP1898) (1)
Toxicity (LD_{50} orally mg/kg)	325 rats (6)

The structure of HAN is shown in Figure 1 and Figure 2. HAN is an ionic liquid, which by definition is a compound with a melting temperature below the boiling point of water (14). As indicated by the name ‘ionic’, HAN exhibits strong ion-ion interactions. $[NH_3OH]^+$ is the cation

and $[NO_3]^-$ acts as the anion. $[NO_3]^-$ molecule has a resonance structure as shown in Figure 1, where 2 electrons are shared between 3 *N-O* bonds.

Table 4. Density and Specific Heat of HAN-Water Solutions (15)

HAN Concentration	Density (kg/m^3)	Specific heat (J/kg^0C)
13.0M	1537	1570
10.7	1449	1553
9.0M	1382	1733

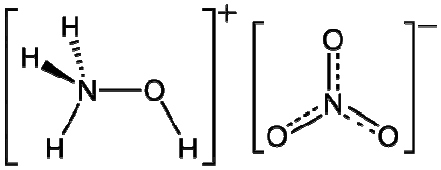

Figure 1. Molecular Structure of HAN

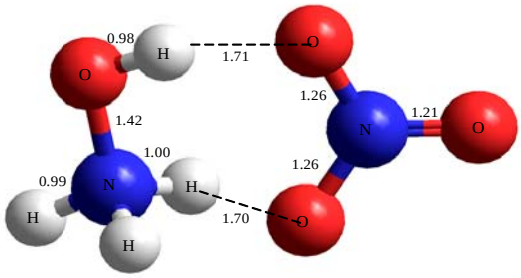

Figure 2. Gas-phase optimized structure of HAN (16)

Burning of water solutions of HAN, $NH_2OH.HNO_3$, was first described in the open literature by R.H Comer in 1976 (17). This work was devoted to the development of liquid gun

propellants, which was of deep concern to defense scientists and engineers for several decades. In this work, the abnormal dependence of the burning rate on pressure within the pressure range p = 40-80 MPa, the burning rate tended to decrease with increasing pressure.

In the late 1980s, S. R. Vosen studied the burning of water solutions of HAN and HAN/TEAN (triethanolamine nitrate) (18). He confirmed the strong positive influence of the effective diameter of the tube and the negative influence of pressure on the burning rate of water solutions of HAN. The experiments were conducted in a strand-type burner placed in a large vessel. The open top strand burner had a cross section of 1.8 x 1.0 mm^2, and a liquid depth of 40 mm, defining a volume of 72 x 10^{-9} m^3. HAN-water solutions of 3.12M, 5.20M, 7.02M, 9.10M, 11.05M, 13.00M, and LP1845 (34.5/4.9/60.3 : HAN/TEAN/H_2O) were used in the study. Figure 3 shows the variation of the apparent mass decomposition rate of various HAN-water solutions with pressure. The apparent mass burning rate is defined in the study as:

$$\dot{m}'' = \rho_1 S_u A_d / A_b$$

where $\dot{m}''$ is the apparent mass burning rate, ρ_1 is the liquid density, S_u is the linear decomposition rate, A_d is the decomposition area, and A_b is the burner cross section area.

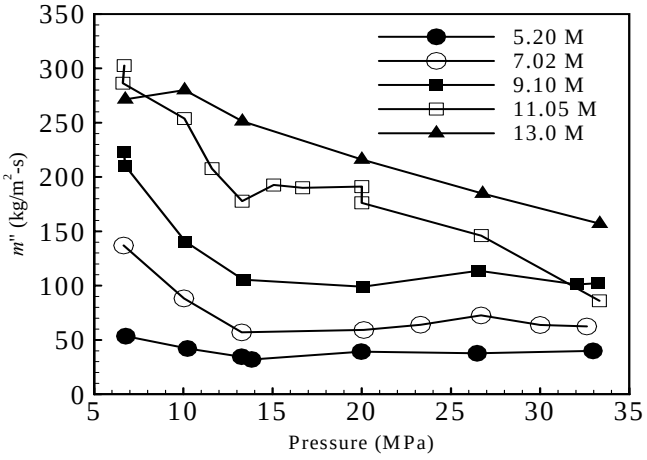

Figure 3. Apparent mass decomposition rate of HAN-water mixtures as a function of pressure (18)

It was found that 3.12M HAN could not sustain a decomposition wave even with electric discharge of as much as 10J. It is seen from Figure 3, that for solutions of 5.20, 7.02, and 9.10M HAN, $\dot{m}''$ first decreases till about 13MPa, then becomes independent of pressure. High-speed cineshadowgraphy was used to capture the decomposition phenomenon. The abnormal behavior of burning rates at p < 13MPa can be explained by considering the expression of the apparent mass decomposition rate. At low pressures the interface has a large meniscus with small corrugations, larger meniscus corresponds to larger decomposition area and hence a larger apparent mass decomposition rate. As the pressure is increased, the meniscus becomes less and less pronounced, becoming indiscernible at pressures above 13MPa and hence the apparent decomposition rate decreases. The apparent decomposition rate for 11.05 and 13.00 M HAN solutions shows a different trend, it decreases monotonically with pressure. Their interface shape is similar to that of 5.20 to 9.10 M HAN mixtures at pressures below 13MPa.

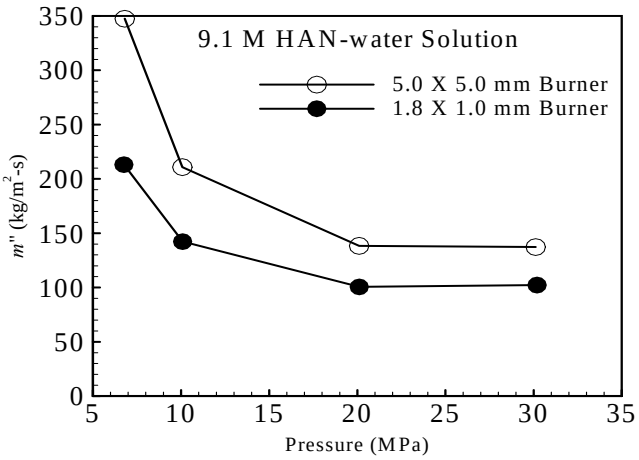

Figure 4. Apparent mass decomposition rate of 9.10M HAN-water solution as a function of pressure and burner size (18)

Figure 4 shows the variation of mass decomposition rate with pressure and burner size. It was seen that the apparent mass decomposition rate increases with burner size.

Solid crystalline HAN was studied by Kondrikov et al. (19). Studies were conducted on HAN and its water solutions in a constant-pressure bomb within a pressure range of 0.1MPa to 36MPa. The test results concluded that solid crystalline HAN was not capable of self-sustained burning at atmospheric pressure. When ignited by a hot Nichrome wire, a slow layer-by-layer decomposition followed an abundant foam evolution. For p = 0.3 MPa, the decomposition was found to be of self-sustaining nature but the velocity was unusually low, only about 50 μm/sec. It was also found that in contrast to water solutions of HAN and HAN-based liquid propellants, the burning rate of the solid substance propagates steadily up to p = 20 MPa after which it rapidly increases with pressure. The pressure exponent in Vielle's law is 1.6 upto 1.1 MPa, becomes as high as 2.6 at $1.1 < p < 2.1$ MPa, and decreases to 1.5 within the interval p = 2.1-2.3.

Chang et al. (5) studied the combustion behavior of XM46, 63.2% HAN, 20.0% TEAN (fuel), and 16.8% water. It was found that the flame structure was demarcated by three different stages: 1) nearly simultaneous decomposition of both HAN and TEAN initiating the liquid to produce gases around 300^{o}C, 2) breakdown of heavy opaque intermediate molecules into transparent species above the burning surface, and 3) reaction of transparent species to form final products in the luminous flame. It was also found that the type of fuel ingredient in HAN-based liquid monopropellant could have a significant effect on the overall burning characteristics. This was studied by taking another HAN-based propellant, consisting of 60 wt% HAN, 14 wt% glycine, and 26 wt% water. The weight fractions of HAN and water in this propellant were comparable to XM46, and the only significant change was the replacement of TEAN by glycine. It was found that within a pressure range of 1.4-7 MPa, the burning rate was lower than that of

XM46 by two orders of magnitude showing the dependence of burning rate on the fuel ingredient.

Fourier Transform Infrared (FTIR) spectroscopy was used to identify thermal decomposition products of water solutions of HAN at atmospheric pressure in nitrogen environment (20). The major species were found to be H_2O, N_2O, NO, NO_2 and HNO_3. It was found that solid HAN had similar decomposition products but the induction times of solid HAN were found to be much larger as compared to HAN-water solution at low initial set temperatures. Thermal decomposition studies of HAN were also carried out using confined rapid thermolysis / FTIR spectroscopy by Kim et al. (21). It was found that proton transfer is probably the dominant mechanism in the formation of HNO_3 which subsequently decomposes to form nitronium (NO_2^+) and hydroxyl (OH^-) ions which are active in the condensed phase.

$$[NH_3OH]^+[NO_3]^- \ (13M) \rightarrow NH_2OH + HNO_3$$

$$HNO_3 \rightarrow NO_2^+ + \ OH^-$$

These ions further react to produce HNO and HONO which appear in wide variety of reaction steps and pathways and hence were considered important in the development of a reaction mechanism of HAN.

Chemical kinetic study of HAN decomposition was carried out by Lee et al. (22) where they proposed a reduced reaction model for HAN decomposition. Experiments were conducted on 13, 10.7 and 9 M HAN. The gas-phase concentrations of the various species were measured using FTIR spectroscopy and the condensed phase reaction temperatures were also measured. Further, an inverse-based analysis was used to deduce the Arrhenius-type reaction rates for the

reduced model using the measured gas-phase concentrations and condensed-phase reaction temperatures as input to the numerical model.

Laser assisted experiments were conducted by Lee et.al (23) to investigate the combustion characteristics of HAN-based liquid propellant, XM46, and its ingredients, HAN and triethanol ammonium nitrate (TEAN). Experiments were conducted over pressure range of 0.1 to 1 atmosphere and heat fluxes from 50 to 400 W/cm^2. A sample 0.2-0.3 cm^3 for XM46 and HAN, and 0.15-0.2 g for TEAN, was held in a small glass container for each test. HAN used in this study was 13 M HAN-water solution, TEAN was solid in a crystalline state, and XM46 was LGP1845, a mixture of HAN, TEAN, and water with the weight ratio of 63.2:20.0:16.8. The sample was fixed in space, and the measurement of gas-phase species or temperature was made at a fixed location above the sample surface. In an actual experiment, initial sample heights were 5-10mm.

Experiments on 13M HAN-water solutions showed that ignition time delay varied in the range of 3.0-4.5 seconds in air environment and between 2.5-5 seconds in an inert (Ar) environment. There is a relatively little change in the ignition time delay since HAN is oxygen-rich and the extra oxygen in air makes no difference in the HAN burning behavior. However, for stoichiometric XM46 and fuel-rich TEAN, the presence of oxygen and change of environment significantly affected their ignition time delays. Table 5 summarizes the ignition time delay for the three materials. Ignition during this study was defined as the first appearance of visible light emission.

Table 5. Comparison of the ignition delay time from first visible light emission in air and argon environments at 400 W/cm2 and 1 atmospheric pressure (Unit: second) (23)

Material	Air Environment	Argon Environment
HAN (13M)	3.0-4.5	2.5-5.0
TEAN	~1.0	2.5-3.5
XM46 (63.2% HAN, 20.0% TEAN, 16.18% H_2O)	1.0-2.7	2.7-4.0

In addition to thermally-induced decomposition of the HAN-based propellants, HAN decomposition by electrolysis has recently been suggested as a viable alternative for applications in microscale thrusters (24), since thermal management for HAN decomposition would be very difficult to control in these small propulsion devices. The other potential benefits of the electrolytic-induced decomposition of HAN-based liquid propellants include low ignition temperature, reduced power requirement, enhanced system durability and reliability, and reduced cost (24). Experiments were conducted on XM46 (60.8 wt% HAN, 19.2 wt% TEAN (triethanolammonium nitrate), and 20 wt% H_2O) to elucidate the electrolytic characteristics of XM46 using microfin electrode module. To develop the microfin electrode, first, prototype electrodes consisting of a Teflon screen sandwiched between two stainless steel meshes that were attached to a voltage source were examined (Figure 5, left) to ensure the feasibility of the electrolytic ignition concept. Experiment, were conducted using these Teflon electrodes and it was found that the propellant initially bubbled at the surface of electrodes and then gasification occurs to establish a self-propagating thermal wave. The results were comparable to published results (25).

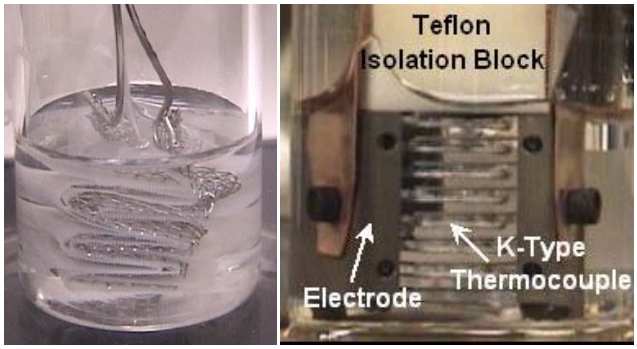

Figure 5. Comparison of prototype electrodes with titanium microfin electrodes (26)

Based on the feasibility result from the initial experiments, microfin electrodes were fabricated (Figure 5, right). The Titanium microfin electrode consisted of 8 parallel fins (19 X 9 X 0.25 mm) at a distance of 1 mm each. The input voltage to the electrodes ranged from 7 to 26 VDC and the microfin electrode surface area ranged from 1050 to 4200 mm^2. Fin surface area was varied by changing the submersion depth of the electrodes in the liquid propellant. A schematic diagram of the experimental setup is shown in Figure 6. The experiment was conducted by submerging the microfin electrode in 15 ml of the liquid propellant to a specified depth depending on the desired electrode surface area for the test. Voltage was then applied across the electrodes in the range of 0-40 V at a current beyond 35 A. The decomposition process was carefully monitored and as the current reached the peak value, input voltage was removed. The decomposition process continued until the mixture was diluted with water to terminate the test. During the test, electrode amperage, electrode voltage, and liquid temperature were measured as a function of time. The liquid resistance, power, and energy loads were then evaluated. The electrolytic ignition concept was demonstrated successfully to gasify HAN-based liquid propellants, specifically XM46. It was also found that the decomposition temperature of XM46 was 115^oC at room temperature and that it was independent of the input voltage.

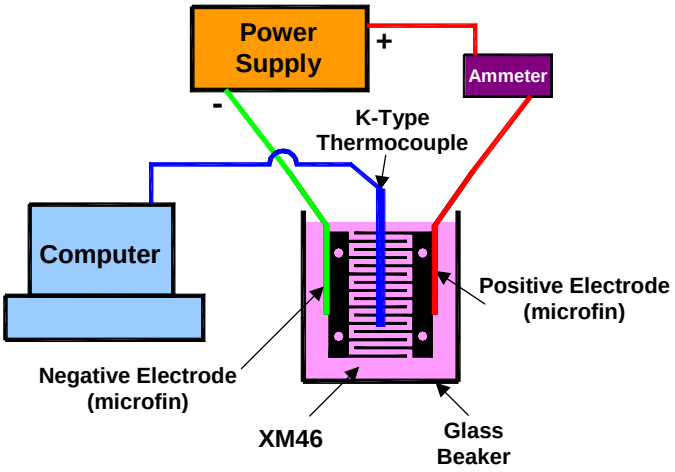

Figure 6. Experimental diagram using microfin electrodes (HAN decomposition at low heating rates) (26)

The objective of this research is to study the electrolytic induced ignition of HAN. The purpose is to identify the various parameters and mechanisms dictating the electrolysis of HAN-based monopropellants. Thermal decomposition mechanisms from Lee et al. (22) are used along with electrochemical mechanisms to simulate the ignition phenomenon. Ignition is characterized by temperature run away in the temporal evolution of temperature. The ignition of HAN-water solution by electrolysis is then treated numerically using a constant pressure homogeneous reactor model. A stiff ODE solver is used in the analysis to handle the highly stiff species conservation and the energy equations. Temporal evolution of temperature and condensed and gas phase species are then studied to explain the highly complex phenomenon of HAN-water solution. Parametric studies involving electric current, voltage, volume, initial temperature, and HAN concentration are performed to see their effect on the ignition time delay.

2 Electrochemical and Chemical Mechanisms

A simple schematic for HAN decomposition by electrolysis is illustrated in Figure 7. Electric current has been applied to initiate the process. Based on fundamental electrochemical theories, liquid water would be electrolyzed, leading to the following electrochemical reaction on the anode side:

$$H_2O \rightarrow \frac{1}{2}O_2 + 2H^+ + e^- \quad \text{(R1)}$$

The proton produced in this electrolysis process promotes the following HAN decomposition reaction:

$$(NH_3OH)^+ (NO_3)^- + H^+ \rightarrow HNO_3 + (NH_3OH)^+ \quad \text{(R2)}$$

Combining steps (R1) and (R2) leads to an overall electrochemical reaction on the anode side:

$$2\,(NH_3OH)^+ (NO_3)^- + H_2O \rightarrow \frac{1}{2}O_2 + 2\,HNO_3 + 2\,(NH_3OH)^+ + 2\,e^- \quad \text{(R3)}$$

Since the ion, $(NH_3OH)^+$, exists in high concentration in the HAN-water solution, it can easily migrate to the cathode side and become reduced by the electron, which arrives at the cathode through the outside circuit. This leads to the following electrochemical-reduction reaction on the cathode side:

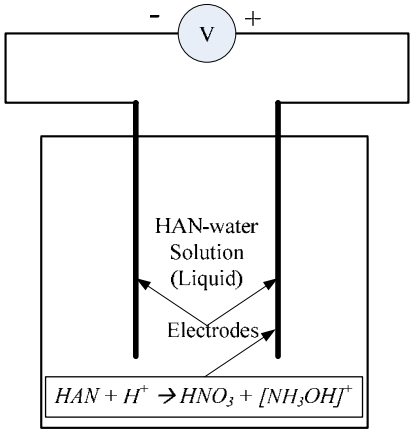

Figure 7. Schematic of HAN decomposition by electrolysis

$$2\,(NH_3OH)^+ + 2\,e^- \rightarrow 2\,NH_2OH + H_2 \qquad \text{(R4)}$$

Based on steps (R3) and (R4), the global reaction arising from the electrolysis becomes:

$$2\,(NH_3OH)^+\,(NO_3)^- + H_2O \rightarrow 2\,HNO_3 + 2\,NH_2OH + H_2 + \frac{1}{2}O_2 \qquad \text{(R5)}$$

The electrolysis of the HAN-water solution thus produces two species, HNO_3 and NH_2OH, which subsequently open up a series of reactions. Reaction, (R5), is very similar to the first and rate-limiting step of a series of chemical reactions during the thermal decomposition of HAN (22), as presented in (R6) in the following paragraph.

In addition to the anodic and cathodic electrochemical reactions, as given in steps (R3) and (R4), thermal decomposition of HAN is considered for accurate account of HAN decomposition by electrolysis. These reactions are (22):

$$HAN + H_2O \rightarrow NH_2OH + HNO_3 + H_2O \qquad \text{(R6)}$$

$$NH_2OH + HNO_3 \rightarrow HONO + NHO + H_2O \qquad \text{(R7)}$$

$$NH_2OH + HONO \rightarrow N_2O + 2\,H_2O \quad \text{(R8)}$$

$$NH_2OH + HNO \rightarrow N_2 + 2\,H_2O \quad \text{(R9)}$$

$$3\,HONO \rightarrow 2\,NO + HNO_3 + H_2O \quad \text{(R10)}$$

$$2\,HNO \rightarrow N_2O + H_2O \quad \text{(R11)}$$

$$HNO + HNO_3 \rightarrow 2\,HONO \quad \text{(R12)}$$

$$HONO + HNO_3 \rightarrow 2\,NO_2 + H_2O \quad \text{(R13)}$$

$$(k_{l\rightarrow g})_{N_2O,N_2,NO,NO_2} \quad \text{(R14)}$$

$$(k_{l\rightarrow g})_{H_2O} \quad \text{(R15)}$$

$$(k_{l\rightarrow g})_{HNO_3} \quad \text{(R16)}$$

Therefore in the condensed phase, a total of 10 electrochemical and chemical reactions, (R3), (R4), and (R6)-(R13), are included in the present analysis, involving 12 species, namely HAN, *NH_2OH, HNO_3, HONO, HNO, N_2O, N_2, NO, NO_2, H_2O, H_2*, and *O_2*. Among them, H_2 and O_2 appear only in the gaseous phase. In addition, *HNO_3, N_2O, N_2, NO, NO_2*, and *H_2O*, may evaporate and exist in both the condensed and gaseous phases represented by the reactions (R14)-(R16). The existence of gaseous *H_2* and *O_2* significantly enhance the ignition and combustion of HAN-based propellants. This clearly indicates an advantage of decomposing HAN-based propellants by electrolysis. The reaction rates and activation energies of the reduced condensed phase chemical reactions used in the analysis are listed in Table 6 below (22).

Table 6. Reaction Rates and Activation Energies (22)

Reaction	A	E
$HAN + H_2O \rightarrow NH_2OH + HNO_3 + H_2O^{**}$	1.7 e10 ± 9.3 e2	15.1 ± 0.5
$NH_2OH + HNO_3 \rightarrow HONO + NHO + H_2O^{**}$	3.7 e4 ± 8.9 e3	6.6 ± 0.7
$NH_2OH + HONO \rightarrow N_2O + 2\,H_2O^{**}$	7.8 e4 ± 4.5 e3	3.3 ± 0.2
$NH_2OH + HNO \rightarrow N_2 + 2\,H_2O^{**}$	1.5 e5 ± 2.4 e2	2.7 ± 0.1
$3\,HONO \rightarrow 2\,NO + HNO_3 + H_2O^{***}$	1.5 e13 ±5.3 e2	9.1 ± 0.2
$2\,HNO \rightarrow N_2O + H_2O^{**}$	7.5 e13 ± 58	17.1 ± 0.1
$HNO + HNO_3 \rightarrow 2\,HONO^{**}$	7.5 e8 ± 0.3	16.6 ± 0.1
$HONO + HNO_3 \rightarrow 2\,NO_2 + H_2O^{**}$	0.3 ± 1.8 e2	0.7 ± 0.1
$(k_{l\rightarrow g})_{N_2O,N_2,NO,NO_2}$	2.7 e3 ± 5.9	2.4 ± 0.1
$(k_{l\rightarrow g})_{H_2O}$	3.9 e5 ± 1.1 e2	9.9 ± 0.1
$(k_{l\rightarrow g})_{HNO_3}$	3.6 e5 ± 2.0 e3	12.8 ± 0.6

Unit of A: * 1/sec, ** $(cm^3/mol)/sec$, *** $(cm^3/mol)^2/sec$, Unit of E: (kcal /mol)

The gaseous species produced by the condensed phase reactions subsequently opens up a series of gas phase reactions. A total of 32 species and 151 reactions in gaseous phase are considered for the study. The list of species and reactions considered in gas phase is shown in Appendix A.

3 Theoretical Formulation

The physical problem under study is the ignition of HAN-water monopropellant induced by the application of electric current. The problem is modeled as a constant pressure, adiabatic, homogeneous reactor. The detailed physiochemical processes involved are schematically illustrated in Figure 8. The liquid propellant is initially at some defined temperature. Once potential difference is applied across the electrodes, the HAN-water solution dissociates due to its ionic nature. After this dissociation reaction, a series of reactions, as well as phase transition reactions (R14)-(R16) start in the condensed phase generating bubbles, water vapor being the major product (Figure 8b). The initial vaporization reactions lead a series of gaseous phase reactions governed by the H-O-N kinetic scheme consisting of a total of 32 species and 151 reactions (Appendix A). Eventually all the liquid propellant is consumed and ignition takes place in the gas-phase (Figure 8d). The major products are H_2O, N_2, and O_2

3.1 Condensed Phase

3.1.1 Species Conservation Equation

The electrolytic-induced HAN decomposition in (24), shown schematically in Figure 7 is numerically studied. Various key parameters and electrochemical mechanisms dictating the decomposition process are explained. The analysis is based on the assumption of a homogeneous, constant-pressure reactor, and focuses on the temporal evolution of the 10 species in the condensed phase.

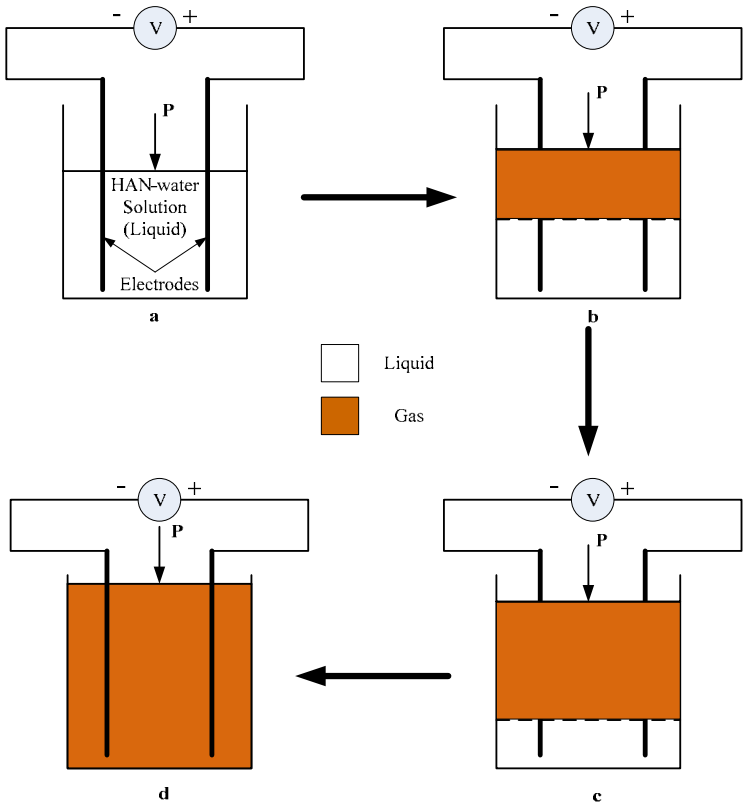

Figure 8. Physiochemical processes involved in electrolytic induced ignition of HAN based monopropellant

$$\frac{d(m_c Y_i)}{dt} = -\delta_i \frac{s_i I}{nF} MW_i + \dot{\omega}\, MW_i\, V_c - k_{l\to g,i} m_c Y_i \qquad (1)$$

where the three terms on the right hand-side arise from the electrochemical reactions, (R3) and (R4), chemical reactions, (R6)-(R13), and evaporation processes, (R14)-(R16), respectively. The parameters, m_c and V_c, stand for the mass, and volume in the condensed phase, respectively; Y_i, Mw_i, the mass fraction and molecular weight of species i respectively; and t, I, F, the time, electric current, and the Faraday constant (96487 C/mol); respectively. The rate of conversion from the liquid to gas for species i, $k_{l\text{-}g,i}$, can be found in Table 6. The electrolysis term in Equation (1) is formulated in the following general form:

$$\sum_i s_i M_i = n\, e^- \tag{2}$$

where the parameter, M_i, represents any chemical component in the electrochemical reaction, s_i the stoichiometric number, and n the number of electrons.

The parameter δ_i, in Equation (1) is defined as:

$$\delta_i = \begin{cases} 1 & for\ species\ HAN, HNO_3, NH_2OH, H_2O \\ 0 & for\ all\ other\ species \end{cases} \tag{3}$$

The chemical production rate, $\dot{\omega}$ in Equation (1) is related to the chemical kinetics. For the forward reactions, (R6)-(R13),$\dot{\omega}$ can be derived as:

$$\dot{\omega} = \sum_{j=1}^{M} \nu_{ji} k_j \prod_{i=1}^{N} [x_i]^{\nu'_{ji}} \tag{4}$$

where the parameter, M, stands for the total number of chemical reactions (8 in this case), N the total number of species (10 in the condensed phase).

The parameter ν_{ji} can be expressed as:

$$\nu_{ji} = \nu''_{ji} - \nu'_{ji} \tag{5}$$

where ν'_{ji} and, ν''_{ji} are the stoichiometric coefficients on the reactant and product sides of the chemical reaction, respectively, for the ith species in the jth reaction.

The rate coefficient of the chemical reaction, k_j, can be expressed in the Arrhenius form as:

$$k_j = A_j \exp\left\{\frac{-E_j}{R_u T}\right\} \tag{6}$$

where A_j and E_j are the pre-exponential factor and the activation energy of the jth reaction, which can be found in Table 6. R_u is the universal gas constant, and T the temperature of the condensed phase.

3.1.2 The Energy Equation

For a homogeneous, adiabatic, constant-pressure reactor, the energy equation in condensed phase can be derived as follows:

$$\frac{dH_c}{dt} = -\sum_i \dot{m}_{l\to g,i}\, h_{fg,i} + VI \tag{7}$$

where H_c is the total enthalpy in the condensed phase, V is the voltage applied and the other terms are defined before. The two terms on the right hand-side represent the energy change caused by vaporization, and energy addition by the electrolysis process, respectively.

Now, the total enthalpy in the condensed phase can be written as:

$$H_c = \sum_{ci} m_{ci} \left(h_{ci}^0 + \int C_{p,ci} dT\right) \tag{8}$$

Therefore,

$$\frac{dH_c}{dt} = \sum_{ci} \frac{dm_{ci}}{dt} \left(h_{ci}^0 + \int C_{p,ci} dT\right) + \left(\sum_{ci} m_{ci}\, C_{p,ci}\right) \frac{dT}{dt} \tag{9}$$

The term due to evaporation can be further defined as:

$$\sum_i \dot{m}_{l\to g,i}\, h_{fg,i} = \sum_i k_{l\to g,i}\; m_{ci}\, h_{fg,i} \tag{10}$$

Based on the preceding derivation, Equation. (7) can finally be written as:

$$C_{p,c}\,\frac{dT}{dt} = -\sum_{ci}\frac{dm_{ci}}{dt}\left(h_{ci}^{0} + \int C_{p,ci}dT\right) - \sum_{i} k_{l\rightarrow g,i}\; m_{ci}\, h_{fg,i} + VI \qquad (11)$$

The first term on the right hand side is term due to energy released by the chemical reactions, hence equation (11) can be written as:

$$C_{p,c}\,\frac{dT}{dt} = -\sum_{ci}\dot{\omega} MW_i V_c\left(h_{ci}^{0} + \int C_{p,ci}dT\right) + \sum_{i} k_{l\rightarrow g,i}\, m_{ci} h_{fg,i} + VI \qquad (12)$$

3.2 Gas Phase

3.2.1 Species Conservation Equation

The reacting mixture is treated as a closed system with no mass crossing the boundary, so the total mass of the gaseous mixture $m = \sum_{k=1}^{K} m_k$ is a constant and *dm/dt* = 0. Here m_k is the total mass of *k*th gaseous species and *K* is the total number of species in the mixture. The individual species are produced or destroyed according to

$$\frac{dm_k}{dt} = V\,\dot{\omega}_k MW_k \quad k = 1,2,\ldots,K \qquad (13)$$

where $\dot{\omega}_k$ is the molar production rate of the *k*th species by elementary reaction, MW_k is the molecular weight of the *k*th species, and *V* is the volume of the system which may vary in time. Since the total mass is constant, this may be written in terms of mass fraction as

$$\frac{dY_k}{dt} = \frac{\dot{\omega}_k MW_k}{\rho} \quad k = 1,2,\ldots,K \qquad (14)$$

where $Y_k = m_k / m$ is the mass fraction of kth species and $\rho = m/V$ is the density. $\dot{\omega}_k$ is calculated as shown in equation (4).

3.2.2 The Energy Equation

According to the first law of thermodynamics for a pure substance in an adiabatic, closed system at constant pressure:

$$dh = 0 \tag{15}$$

where h is the specific enthalpy. This relation is also true for an ideal mixture of gases, with the internal energy of the mixture given by:

$$h = \sum_{k=1}^{K} Y_k \, h_k \tag{16}$$

where h_k is the specific enthalpy of the kth species. Taking the derivative of the above equation yields:

$$dh = \sum_{k=1}^{K} dY_k \, h_k + \sum_{k=1}^{K} Y_k \, dh_k \tag{17}$$

Assuming calorically perfect gases, $dh_k = c_{p,k} \, dT$, where T is the temperature of the mixture and $c_{p,k}$ is the specific heat of kth species evaluated at constant pressure. Defining the mean specific heat of the mixture, $c_p = \sum_{k=1}^{K} Y_k \, c_{p,k}$ and differentiating with respect to time, the energy equation becomes:

$$c_p \frac{dT}{dt} + \frac{1}{\rho} \sum_{k=1}^{K} h_k \dot{\omega}_k MW_k = 0 \tag{18}$$

The set of equations (14) and (18) can be solved simultaneously to obtain temporal evolution of species mass fraction and temperature in the gas phase.

Numerically, for each time step, the gas phase species generated in the condensed phase are fed as initial conditions for the gas phase reactions. The updated species mass fraction and the temperature in the gas phase is then given as feedback to the condensed phase for the next time step and this process is repeated till the end of computational time for each time step. A flow chart of the program is shown in Appendix B.

4 Numerical Scheme

An initial value ODE solver for stiff and non-stiff systems, VODE (variable coefficient ordinary differential equation solver) (27) is used for solving the coupled species conservation equation and the energy equation. VODE uses variable-coefficient Adams-Moulton and backward differentiation formulas (BDF) methods in Nordsieck form, as taken from the older solvers EPISODE (28) and EPISODEB (29), treating the Jacobian as full or banded.

Stiffness in a system of ordinary differential equations is difficult to characterize precisely. However, it is typical of stiff ODEs that the Jacobian matrix *J (u,t)*, whose element in row *i* and column *j* is

$$J^{ij}(u,t) = (\partial F^i/\partial Y^j)\,(u,t)$$

has one or more eigenvalues whose real parts are negative and large in modulus. As a result, the solution has one or more terms which decay very rapidly in comparison to other terms present. An example of stiff system is (30)

$$\dot{Y}(t) = \begin{bmatrix} 998 & 1998 \\ -999 & -1999 \end{bmatrix} Y(t), \qquad Y(0) = \begin{bmatrix} 1 \\ 0 \end{bmatrix}$$

for which the exact solution is

$$Y(t) = \begin{bmatrix} 2 & -1 \\ -1 & 1 \end{bmatrix} \begin{bmatrix} \exp(-t) \\ \exp(-1000t) \end{bmatrix}$$

and the eigenvalues of the Jacobian are *-1000* and *-1*. The full description of the method is given in (31). An abridged version of the method is given below in the following paragraphs.

The initial value problem can be written as

$$\dot{y} = \frac{dy}{dt} = f(t, y), \qquad y(t_0) = y_0, \qquad y \in \boldsymbol{R^N}$$

The basic linear multistep formulae for both the stiff and non-stiff cases have the form

$$\sum_{i=0}^{K_1} \alpha_{n,i}\, y_{n-i} + h_n \sum_{i=0}^{K_2} \beta_{n,i}\, \dot{y}_{n-i} = 0$$

For use on non-stiff problems, the Adams formula is characterized by $K_1 = 1$ and $K_2 = q - 1$, and the order q varies between 1 and 12. For stiff problems, the BDF formula has $K_1 = q$ and $K_2 = 0$, and the order of q varies between 1 and 5. The coefficients $\alpha_{n,i}$ and $\beta_{n,i}$ are computed as functions of the current and past step sizes $h_j = t_j - t_{j-1}$ $(j = n-q+1, \ldots n)$. The past history is represented by the $\boldsymbol{N}$ by $q+1$ Nordsieck array,

$$z_n = \left[y_n, h_n\, \dot{y}_n, \ldots, h_n^q \frac{y_n^{(q)}}{q!} \right]$$

the scaled derivatives being those of corresponding interpolation polynomial associated with the history data in the formula.

The method being an implicit method, the iterative scheme applied at each time step to solve the non-linear system of equations is

$$G(y_n) \equiv y_n + h_n(\beta_{n,0}/\alpha_{n,0})\, f(t_n, y_n) + a_n = 0$$

for the advanced value y_n (a_n is a vector involving past values of $y_n$and $\dot{y}_k$). The solvers offers a choice between functional iterations and a modified Newton iteration in which the Jacobian matrix $J = \partial f/\partial y$ is treated as either full or banded. In the Nordsieck representation, the form

$$G(y_n) = y_n - y_{n(0)} - (h_n/l_1)[\, f(t_n, y_n) - \dot{y}_{n(0)}]$$

and the final correction to the Nordsieck array is

$$z_n = z_{n(0)} + [y_n - y_{n(0)}]l$$

in terms of a vector of coefficients $l = [l_0, l_1, \ldots, l_q]$ ($l_0 = 1$).

Following a successful corrector iteration for y_n, the local error is estimated and tested. Regardless of the outcome, a change in step size is considered, either for the current step or the next one, depending on the error test. Periodically, a change in the order q is also considered, based on estimated local errors at orders $q - 1$ and $q + 1$.

5 Results and Discussion

5.1 Condensed Phase Code Validation

The theoretical formulation and computational code are first validated against experimental data in (22) for the species evolution in the condensed phase at isothermal conditions. The electrolytic term in the condensed phase species conservation equation is switched off in this validation study of thermal decomposition. Figure 9 shows the temporal evolution of species concentration of 13M HAN solution, decomposing at isothermal temperatures of 195 ^{0}C. It is evident from the figure that the simulation coincides with the reference data almost exactly. Although the reference experiment was done at an initial set temperature but there was an initial gradient in temperature after which the temperature became steady at 195 ^{o}C. The experimentally measured temperature was curve fitted using a 6*th* order polynomial and an exponential function and was then used for the simulation. The temperature profile is shown in Figure 10.

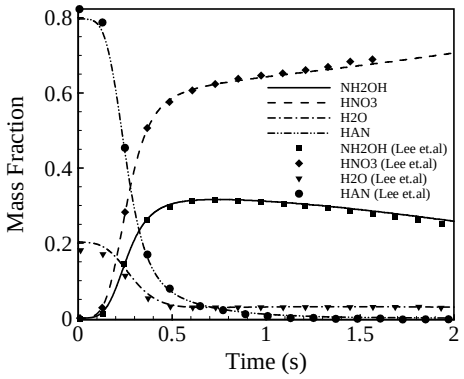

Figure 9. Condensed-phase mass fractions of 13M HAN at set temperature of 195 ^{0}C

The equations of the curves used to fit the temperature are:

$$T = \begin{cases} -157.43t^6 + 322.73t^5 - 1159.10t^4 + 2099.90t^3 - 2014.10t^2 + 951.47t + 310 \ for\ t \le 0.50 \\ 473.99t^{-0.021} \qquad for\ 0.50 < t < 2.0 \end{cases}$$

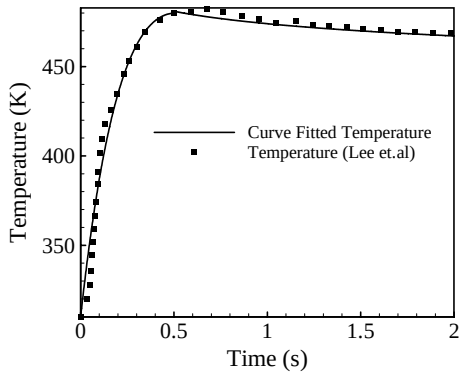

Figure 10. Condensed-phase reaction temperature profile of 13 M HAN at a set temperature of 195 ^{0}C

5.2 Gas Phase Code Validation

The gas-phase code is used to simulate Propane-Air kinetics and verified against CHEMKIN results Figure 11 for the same reaction kinetics. A total of 31 species and 76 reactions are used to for the present case. The species involved and the chemical reactions used are listed in Appendix C. The initial conditions used in both the cases are P = 1atm, T = 1200K and using stoichiometric F/A ratio, i.e., C3H8 : O2 : N2 = 1: 5 : 18.8. The graph shows a very good match for the temporal evolution of temperature.

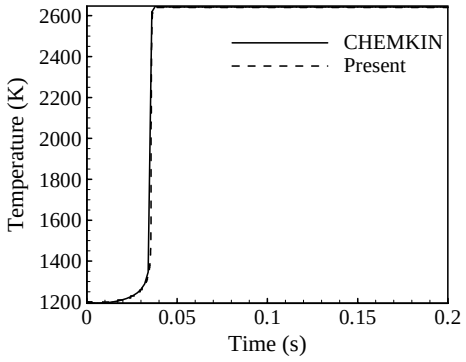

Figure 11. Comparison of temperature evolution

The species evolution for the major as well as key radicals also shows a fairly good match. Figure 12 and Figure 13 shows the evolution of major species as calculated by the gas phase code and CHEMKIN. Figure 14 and Figure 15 shows the temporal evolution of key radicals simulated by the gas phase code and CHEMKIN.

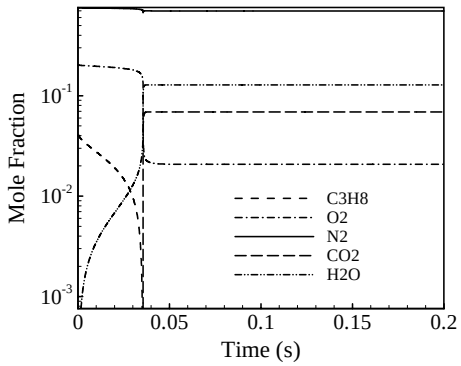

Figure 12. Time evolution of Major Species

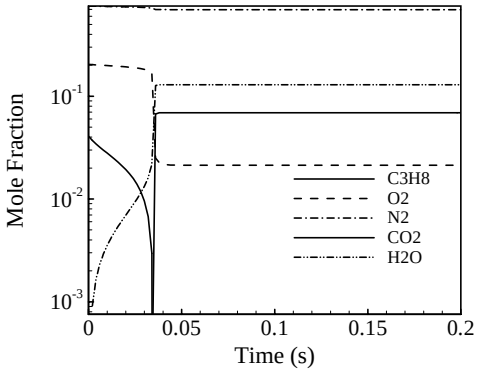

Figure 13. Time evolution of Major Species (CHEMKIN)

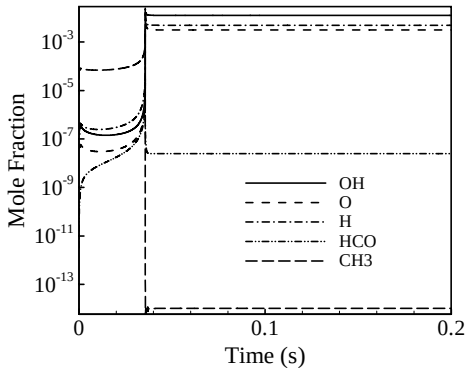

Figure 14. Time evolution of key radicals

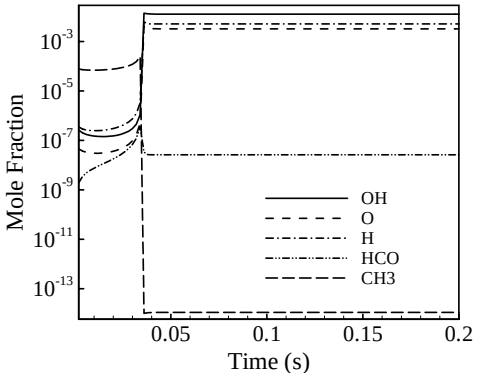

Figure 15. Time evolution of key radicals (CHEMKIN)

5.3 Full Code Validation

The code is validated using ignition time delay data from listed in Table 5 (23). 0.3 cc of 13M HAN-water solution is taken at an initial temperature of 300K and 1 atmosphere pressure.

The energy flux of 400 W/cm^2 used during the experiment is translated into the total power input by a simple calculation involving the volume and height of the test sample. The translated power input for 0.3cc sample with a height of 10mm is calculated to be 120W. Since the amount of energy actually absorbed by the propellant during the laser induced ignition experiment is not known, a parametric study is done varying the total power input from 120W to 72W. For this analysis, the electrolytic term in the condensed-phase species equation is switched off while the source term in the energy equation is kept intact to simulate the laser assisted thermal ignition.

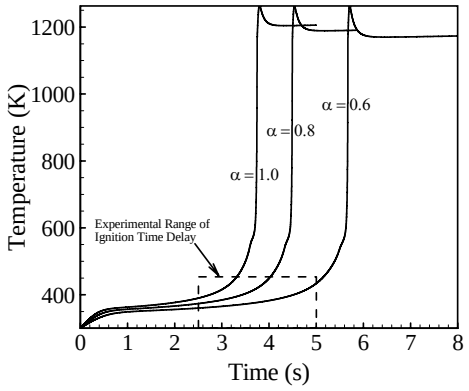

Figure 16. Temperature evolution of 0.3cc 13 M HAN-water solutions at an initial temperature of 300K at various power inputs

The result (Figure 16) shows that the code predicts the ignition time delay with reasonable limits of the experimental data. For power input of 120 and 96 W, the ignition time delay is found to be in the range of experimental data. For a power input of 72W, the ignition time delay calculated by the code is within ~18% of the maximum experimental value of the ignition time delay.

The induction time corresponds mainly to the evaporation of water as shown in Figure 17. Lee et al. (23). Figure 17 also suggests that during the decomposition period, water

vapor is the major decomposition species. This fact is also bolstered by the confined rapid thermolysis/FTIR spectroscopy experiment done on HAN-water solutions by Kim et.al (21).

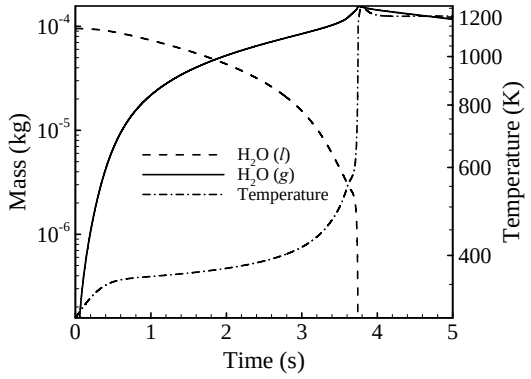

Figure 17. Mass evolution of H_2O (*l*) and H_2O (*g*) at an initial temperature of 300K and a power input of 120W

5.4 Parametric Studies

The effect of initial temperature, current, volume and current is studied on the ignition time delay of electrolytic ignition of HAN-water solution. First the effect of initial temperature is studied. During this analysis, the ignition time delay of 0.1cc of the propellant is calculated at various initial temperatures and current inputs. The results show that the ignition time delay decreases as the initial temperature is increased. It can also be seen from Figure 18 that the ignition time delay varies exponential with the current input.

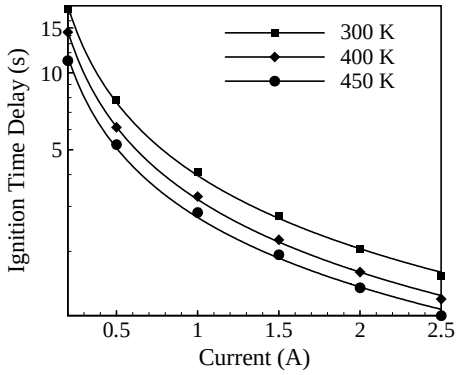

Figure 18. Ignition time delay Vs Current at various initial temperatures

Next, the effect of the total electric current on HAN electrolytic decomposition is studied as shown in Figure 19. As expected, at a specified initial temperature of 350K and a specified initial volume, increasing the total current drastically reduces the HAN ignition time delay.

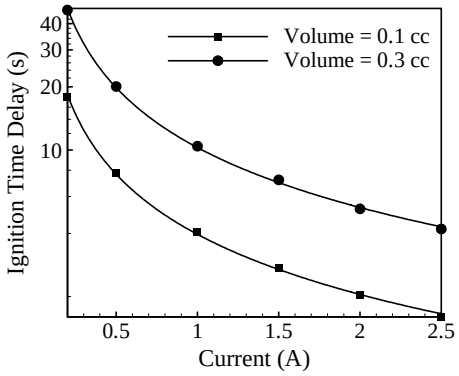

Figure 19. Ignition time delay Vs Current at various initial volumes

Since the electrolytic-induced HAN ignition is intended for propulsion applications in small-scale devices, the volume effect on the ignition process is thus examined. As shown in Figure 19, at an initial temperature of 350 K, a 13M HAN-water solution ignites faster with a smaller volume of 0.1cc under a specified total electric current as compared to a volume of 0.3cc.

The effect of HAN concentration on the ignition time delay is next studied. Figure 20 shows that for 0.1cc of the propellant at an initial temperature of 300K and constant pressure of 1atm, as the concentration is decreased from 13M to 9M, the ignition time delay is increased. This is intuitive since 9M HAN-water solution has a higher water content as compared to 13M HAN-water solution and hence it takes more time for the water to evaporate and hence for ignition to occur.

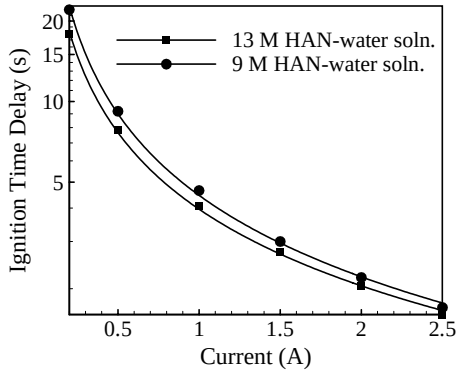

Figure 20. Ignition time delay Vs Current at an initial temperature of 300K and 1atm pressure

6. Conclusion and Future Work

In this work, HAN decomposition and ignition by electrolysis has been studied for applications in small-scale propulsion devices. The relevant electrochemical mechanisms are first established based on the fundamental electrochemical theories. Combining the present electrochemical mechanisms and the prior chemical kinetics, ignition process of HAN by electrolysis is then numerically investigated, focusing on the effects of the electrochemical mechanisms and a number of key parameters on the ignition process. A lumped numerical model has been developed based on an assumption of a homogeneous, constant pressure reactor. Results indicate that the electric current significantly enhances HAN decomposition, comparing with the pure thermal decomposition process. At a constant temperature and a specified initial volume, increasing the total current decreases the ignition time delay of HAN-water solutions. Decreasing the initial volume of the HAN solution also expedites the electrolytic ignition process, indicating that the electrolytically-induced HAN ignition is especially appropriate for applications in small scale propulsion devices. It is also seen that at a constant volume and temperature, a more concentrated solution of HAN ignites faster than a lower concentrated solution if equal electric current is applied. In addition, the gaseous hydrogen and oxygen species produced by electrolysis should be helpful for the subsequent ignition and combustion processes of the HAN-based monopropellants.

Considerable amount of work is needed before the complex behavior of HAN-based propellants can be fully understood, and it is hoped that the present work can be a contribution for further investigations into the decomposition, ignition and combustion of HAN-based propellants. Future work should be directed towards the development of more sophisticated

chemical kinetics, both in liquid and gas phases. In addition to this, rigorous experiments should be conducted to calculate the properties of various species generated during the decomposition/combustion of HAN-based propellants, especially the species generated in the condensed phase. Furthermore, to study the effect of electrolysis, detailed electrolytic kinetic mechanism should be developed and employed to obtain real insight into the electrolytic decomposition of HAN and its variants.

Bibliography

1. Jankovsky, R. S., "HAN-Based Monopropellant Assessment for Spacecrafts," AIAA-96-2863, NASA Technical Memorandum 107287.

2. Jankovsky, R. S., and Oleson, S. R., "HAN-Based Monopropellant Propulsion System With Applications," NASA, 1997. NASA Technical Memorandum107407.

3. Palaszewski, B, Ianovski, L. S. and Carrick, P., "Propellant Technologies: Far-Reaching Benefits for Aeronautical and Space-Vehicle Propulsion," *Journal of Propulsion and Power*, 1998, p. 614.

4. Sackheim, R. L. and Byers, D. C., "Status and Issues Related to In-Space Propulsion Systems," *Journal of Propulsion and Power*, 1998, p. 669.

5. Chang Y.P., et al., "Combustion behavior and flame structure of XM46 liquid propellant," *Journal of Propulsion and Power*, Vol. 17, July–August 2001.

6. Anflo, K, et al., "Towards Green Propulsion for Spacecraft With ADN-Based Monopropellants," AIAA, Indianapolis, Indiana, AIAA-2002-3847.

7. Schmidt, Eckart W., "Hydrazine and its Derivatives : Preparation, Properties, Applications. s.l." Wiley-Interscience, 2001.

8. Gordon, Sanford and McBride, B. J., "Computer Program for Calculation of Complex Chemical Equilibrium Compositions and Applications," NASA, 1994. NASA Reference Publication1311.

9. Palaszewski, Bryan, Ianovski, Leonid S. and Carrick, P., "Propellant Technologies: A Persuasive Wave of Future Propulsion Benefits," NASA, 1997. NASA/TM—97-206228.

10. Mueller, Kurt F and Wagaman, Kerry L. Oxidizing Agent. H001768 United States, January 05, 1999. United States Patent.

11. Courtheoux, Laurence, et al., "Thermal and Catalytic Decomposition of HNF and HAN Liquid Ionic as Propellants," *Applied Catalysis B: Environmental*, Elsevier, 2006, Vol. 62, pp. 217-225.

12. Kuwahara, T, Nakagawa, I, Hatano, H, Onda, T, Takizuka, M., "Thermal Decomposition Characteristics of HAN Composite Propellant," AIAA, 1997, Seattle, WA, AIAA 97-3128.

13. American Chemical Society. http://pubs.acs.org/. [Online] [Cited: October 31, 2008.] http://pubs.acs.org/subscribe/journals/jpcbfk/suppinfo/jp073539t/jp073539tsi20070717_084324.doc?sessid=2395.

14. Wasserscheid, Peter and Welton, T., [ed.], "Ionic Liquids in Synthesis. 2nd Edition. s.l.," WILEY-VCH Verlags GmbH & Co. KGaA, Weinheim, 2008. Vol. 1. ISBN: 978-3-527-31239-9.

15. Lee, H. and Litzinger, T. A., "Thermal Decomposition Of Han-Based Liquid Propellants," *Combustion and Flame*, Elsevier Science Inc., 2001, Vol. 127, pp. 2205-2222.

16. Wei, C., Rogers, W. J., and Mannan, M. S., "Thermal decomposition hazard evaluation of hydroxylamine nitrate," *Journal of Hazardous Materials*, 2006, pp. 163-168.

17. Comer, R. H., "Ignition and combustion of liquid monopropellants at high pressure," *Proc. 16th Int. Symposium on Combustion,"* 1976, pp. 1211 – 1219.

18. Vosen, S. R., "Concentration and Pressure Effects on the Decomposition Rate of Aqueous Hydroxyammonium Nitrate Solutions," *Combustion Science and Technolgy*, Gordon and Breach Science Publishers, Inc, 1989, Vol. 68, pp. 85-99.

19. Kondrikov, B. N., et al., "Burning of Hydroxylammonium Nitrate," *Combustion, Explosion and Shock Waves*, 2000, Vol. 36.

20. Lee H., et al., "Thermal decomposition of HAN–based liquid propellants," *Combustion and Flame*, 2001, Vol. 127, pp. 2205–2222.

21. Kim E.S., et al., "Thermal decomposition studies of energetic materials using confined rapid thermolysis / FTIR spectroscopy," *Combustion and Flame*, 1997, Vol. 110, pp. 239-255.

22. Lee, H. S., and Litzinger, T. A., "Chemical Kinetic Study of HAN Decomposition," *Combustion and Flame*, 1-2, October 2003, Vol. 135, pp. 151-169.

23. Lee, Y. J. and Litzinger, T. A., "Combustion Chemistry Of HAN, TEAN, and XM46," *Combustion Science and Technology*, 1999, pp. 19-36.

24. Risha, G. A., Yetter, R. A. and Yang, V., "Electrolytic-Induced Decomposition and Ignition of HAN-based Liquid Monopropellants," *6th International Symposium in Chemical Propulsion* Santiago, Chile, 2005.

25. Chang, Y.P., and Kuo, K. K., "Assessment of Combustion Characteristics, and Mechanism of a HAN-based Liquid Monopropellant", *37th AIAA/ASME/SAE/ASEE Joint Propulsion Conference & Exhibit*, Salt Lake City, UT, 2001.

26. Risha, G. A., Yetter, R. A. and Yang, V., "Electrolytic-Induced Decomposition and Ignition of HAN-based Liquid Monopropellants," *6th International Symposium in Chemical Propulsion* Santiago, Chile, 2005.

27. Brown, P. N., Byrne, G. D., and Hindmarsh, A. C., "VODE: A Variable Coefficient ODE Solver," *SIAM Journal on Scientific and Statistical Computing*, 1989, pp. 1038-1051.

28. Hindmarsh, A. C. and Byrne, G. D., "EPISODE: An Effective Package for the Integration of Systems of Ordinary Differential Equations," 1977, LLNL Report UCID-30112.

29. Hindmarsh, A. C. and Byrne, G. D., "EPISODEB: An Experimental Package for the Integration of Systems of Ordinary Differential Equations with Banded Jacobians," 1976, LLNL Report UCID-30132.

30. Gear, C. W., "Numerical Initial Value Problems in Ordinary Differential Equations" Prentice Hall PTR, 1971.

31. Byrne, G. D. and Hindmarsh, A. C., "A Polyalgorithm for the Numerical Solution of Ordinary Differential Equations," *ACM Transactions on Mathematical Software*, 1975, Vol. 1, pp. 71-96.

Appendix A

Species considered and chemical mechanism used in gas-phase

Species Considered

1.	HNO3	G	0	63.01287	300	5000	1	3	1
2.	H2NOH	G	0	33.03001	300	4000	3	1	1
3.	HN3O4	G	0	107.02567	300	5000	1	4	3
4.	HNNO2	G	0	61.02017	300	5000	1	2	2
5.	HNNO	G	0	45.02077	300	4000	1	1	2
6.	H2O	G	0	18.01534	300	5000	2	1	0
7.	N2O	G	0	44.01280	300	5000	0	1	2
8.	NO	G	0	30.00610	300	5000	0	1	1
9.	H2	G	0	2.01594	300	5000	2	0	0
10.	O2	G	0	31.99880	300	5000	0	2	0
11.	N2	G	0	28.01340	300	5000	0	0	2
12.	NH3	G	0	17.03061	300	5000	3	0	1
13.	NO3	G	0	62.00490	300	5000	0	3	1
14.	O	G	0	15.99940	300	5000	0	1	0
15.	H	G	0	1.00797	300	5000	1	0	0
16.	OH	G	0	17.00737	300	5000	1	1	0
17.	HO2	G	0	33.00677	300	5000	1	2	0
18.	H2O2	G	0	34.01474	300	5000	2	2	0
19.	N	G	0	14.00670	300	5000	0	0	1
20.	NO2	G	0	46.00550	300	5000	0	2	1
21.	NH	G	0	15.01467	300	5000	1	0	1
22.	NH2	G	0	16.02264	300	5000	2	0	1
23.	NNH	G	0	29.02137	250	4000	1	0	2
24.	HNO	G	0	31.01407	300	5000	1	1	1
25.	HONO	G	0	47.01347	300	5000	1	2	1
26.	N2H2	G	0	30.02934	300	5000	2	0	2
27.	H2NNO	G	0	46.02874	300	4000	2	1	2
28.	H2NO	G	0	32.02204	300	4000	2	1	1
29.	HNOH	G	0	32.02204	300	4000	2	1	1
30.	HNNH	G	0	30.02934	300	5000	2	0	2
31.	N2H3	G	0	31.03731	300	5000	3	0	2
32.	N2H4	G	0	32.04528	300	5000	4	0	2

Gas-phase reactions

(k = A T**b exp(-E/RT))

REACTIONS CONSIDERED	A	b	E
1. H2+M=H+H+M	4.57E+19	-1.4	104000.0
H2 Enhanced by 2.500E+00			
H2O Enhanced by 1.200E+01			
2. O+H2O=OH+OH	2.97E+06	2.0	13400.0
3. O+H2=H+OH	5.06E+04	2.7	6290.0
4. O+O+M=O2+M	6.17E+15	-0.5	0.0
H2 Enhanced by 2.500E+00			
H2O Enhanced by 1.200E+01			
5. H+O2=O+OH	1.94E+14	0.0	16440.0
6. H+O2(+M)=HO2(+M)	4.52E+13	0.0	0.0
Low pressure limit: 0.67000E+20 -0.14200E+01 0.00000E+00			
TROE centering: 0.10000E+01 0.10000E-89 0.10000E+91			
H2 Enhanced by 2.500E+00			
H2O Enhanced by 1.200E+01			
7. H+O+M=OH+M	4.72E+18	-1.0	0.0
H2 Enhanced by 2.500E+00			
H2O Enhanced by 1.200E+01			
8. OH+H2=H2O+H	2.16E+08	1.5	3430.0
9. OH+H+M=H2O+M	2.21E+22	-2.0	0.0
H2 Enhanced by 2.500E+00			
H2O Enhanced by 1.200E+01			

10. HO2+O=O2+OH 1.75E+13 0.0 -397.0

11. HO2+H=H2+O2 6.62E+13 0.0 2130.0

12. HO2+H=OH+OH 1.69E+14 0.0 874.0

13. HO2+OH=H2O+O2 1.90E+16 -1.0 0.0

14. HO2+HO2=H2O2+O2 4.20E+14 0.0 11980.0

Declared duplicate reaction...

15. HO2+HO2=H2O2+O2 1.30E+11 0.0 -1629.0

Declared duplicate reaction...

16. H2O2(+M)=OH+OH(+M) 2.95E+14 0.0 48460.0

Low pressure limit: 0.12000E+18 0.00000E+00 0.45500E+05

TROE centering: 0.50000E+00 0.10000E-89 0.10000E+91

17. H2O2+O=OH+HO2 9.64E+06 2.0 3970.0

18. H2O2+H=H2O+OH 1.00E+13 0.0 3590.0

19. H2O2+H=HO2+H2 4.82E+13 0.0 7950.0

20. H2O2+OH=H2O+HO2 1.00E+12 0.0 0.0

Declared duplicate reaction...

21. H2O2+OH=H2O+HO2 5.80E+14 0.0 9557.0

Declared duplicate reaction...

22. N+H2=H+NH 1.60E+14 0.0 25140.0

23. N+O2=NO+O 6.40E+09 1.0 6280.0

24. N+OH=NO+H 3.80E+13 0.0 0.0

25. N+HO2=NH+O2 1.00E+13 0.0 2000.0

26. N+HO2=NO+OH 1.00E+13 0.0 2000.0

27. N+NO=N2+O 3.27E+12 0.3 0.0

28. N+NO2=NO+NO 4.00E+12 0.0 0.0

29. N+NO2=N2O+O 5.00E+12 0.0 0.0

30. N+HNO=NH+NO 1.00E+13 0.0 2000.0

31. N+HNO=N2O+H 5.00E+10 0.5 3000.0

32. N+N2O=N2+NO 1.00E+13 0.0 19870.0

33. NO+M=N+O+M 9.64E+14 0.0 148400.0

N2 Enhanced by 1.500E+00

34. NO+OH(+M)=HONO(+M) 1.99E+12 -0.1 -721.0

Low pressure limit: 0.50800E+24 -0.25100E+01 -0.67560E+02

TROE centering: 0.62000E+00 0.10000E-89 0.10000E+91

H2O Enhanced by 8.300E+00

N2O Enhanced by 5.000E+00

N2 Enhanced by 1.000E+00

Declared duplicate reaction...

35. NO+OH+M=HONO+M 5.08E+23 -2.5 -68.0

Declared duplicate reaction...

36. HO2+NO=NO2+OH 2.11E+12 0.0 -479.0

37. NO2(+M)=NO+O(+M) 7.60E+18 -1.3 73290.0

Low pressure limit: 0.25000E+29 -0.32700E+01 0.74800E+05

TROE centering: 0.95700E+00 0.10000E-89 0.83320E+04

N2O Enhanced by 1.500E+00

H2O Enhanced by 4.400E+00

N2 Enhanced by 1.000E+00

38. NO2+O=O2+NO 3.91E+12 0.0 -238.0

39. NO2+O(+M)=NO3(+M) 1.33E+13 0.0 0.0

Low pressure limit: 0.14900E+29 -0.40800E+01 0.24670E+04

TROE centering: 0.82600E+00 0.10000E-89 0.31910E+04

40. NO2+H=NO+OH 1.32E+14 0.0 361.6

41. NO2+OH(+M)=HNO3(+M) 2.41E+13 0.0 0.0

Low pressure limit: 0.64200E+33 -0.54900E+01 0.23500E+04

TROE centering: 0.83700E+00 0.10000E-89 0.16570E+04

42. NO2+NO2=NO3+NO 9.64E+09 0.7 20920.0

43. NO2+NO2=2NO+O2 1.63E+12 0.0 26120.0

44. NH+M=N+H+M 2.65E+14 0.0 75510.0

45. NH+O2=HNO+O 3.89E+13 0.0 17890.0

46. NH+O2=NO+OH 7.60E+10 0.0 1530.0

47. NH+O=NO+H 5.50E+13 0.0 0.0

48. NH+O=N+OH 3.72E+13 0.0 0.0

49. NH+OH=HNO+H 2.00E+13 0.0 0.0

50. NH+OH=N+H2O 5.00E+11 0.5 2000.0

51. NH+N=N2+H 3.00E+13 0.0 0.0

52. NH+NO=N2O+H 2.94E+14 -0.4 0.0

Declared duplicate reaction...

53. NH+NO=N2O+H ******** -0.2 0.0

Declared duplicate reaction...

54. NH+NO2=NO+HNO 1.00E+11 0.5 4000.0

55. NH+NH=N2+H+H 5.10E+13 0.0 0.0

56. NH2+O2=HNO+OH 1.78E+12 0.0 14900.0

57. NH2+O=HNO+H 6.63E+14 -0.5 0.0

58. NH2+O=NH+OH 6.75E+12 0.0 0.0

59. NH2+H=NH+H2 6.92E+13 0.0 3650.0

60. NH2+OH=NH+H2O 4.00E+06 2.0 1000.0

61. NH2+N=N2+2H 7.20E+13 0.0 0.0

62. NH3+M=NH2+H+M 2.20E+16 0.0 93470.0

63. NH3+O=NH2+OH 9.40E+06 1.9 6460.0

64. NH3+H=NH2+H2 6.40E+05 2.4 10170.0

65. NH3+OH=NH2+H2O 2.04E+06 2.0 566.0

66. NH3+HO2=NH2+H2O2 3.00E+11 0.0 22000.0

67. NH2+HO2=NH3+O2 1.00E+13 0.0 0.0

68. NH2+NH2=NH3+NH 5.00E+13 0.0 10000.0

69. NNH+M=N2+H+M 1.00E+14 0.0 3000.0

70. NNH+H=N2+H2 1.00E+14 0.0 0.0

71. NNH+OH=N2+H2O 5.00E+13 0.0 0.0

72. NNH+NH=N2+NH2 5.00E+13 0.0 0.0

73. NNH+NH2=N2+NH3 5.00E+13 0.0 0.0

74. HNO+O2=NO+HO2 1.00E+13 0.0 25000.0

75. HNO+O=OH+NO 1.81E+13 0.0 0.0

76. HNO+H=H2+NO 1.81E+13 0.0 993.5

77. HNO+OH=H2O+NO 1.00E+13 0.0 993.5

78. HNO+NO=N2O+OH 2.00E+12 0.0 26000.0

79. HNO+NO2=HONO+NO 6.02E+11 0.0 1987.0

80. HNO+NH2=NO+NH3 2.00E+13 0.0 1000.0

81. HONO+O=OH+NO2 1.20E+13 0.0 5961.0

82. HONO+H=H2+NO2 1.20E+13 0.0 7352.0

83. HONO+OH=H2O+NO2 1.26E+10 1.0 135.1

84. N2O+M=N2+O+M 1.30E+11 0.0 59610.0

85. N2O+O=O2+N2 1.00E+14 0.0 28000.0

86. N2O+O=2NO 1.00E+14 0.0 28000.0

87. N2O+H=N2+OH 2.53E+10 0.0 4550.0

Declared duplicate reaction...

88. N2O+H=N2+OH 2.23E+14 0.0 16750.0

Declared duplicate reaction...

89. N2O+OH=HO2+N2 2.00E+12 0.0 40000.0

90. N2O+NO=NO2+N2 1.00E+14 0.0 50000.0

91. HNO3+OH=NO3+H2O 7.80E+10 0.0 0.0

92. NO2+HO2=HONO+O2 4.64E+11 0.0 479.0

93. NH3+NO2=NH2+HONO 5.00E+12 0.0 29500.0

94. NO+NO=N2+O2 1.30E+14 0.0 75630.0

95. NH3+O=H2+HNO 1.10E+10 0.0 500.0

96. NH2+NO=N2+OH+H 1.08E+11 0.0 -1300.0

97. NH+H2O=HNO+H2 1.00E+11 0.5 3000.0

98. NO+N2H2=HNO+NNH 5.00E+12 0.0 10000.0

99. N2+HO2=NO+HNO 7.90E+08 0.5 44800.0

100. NH3+HONO=H2NNO+H2O 8.07E+04 1.9 32725.0

101. NH2+NO2=H2NO+NO 6.56E+16 -1.5 268.0

102. H2NO+H=HNO+H2 3.00E+07 2.0 2000.0

103. H2NO+H=NH2+OH 5.00E+13 0.0 0.0

104. H2NO+M=H2+NO+M 7.83E+27 -4.3 60306.0

105. H2NO+M=HNO+H+M 1.69E+32 -5.0 62312.0

106. H2NO+M=HNOH+M 4.46E+30 -3.8 56888.0

107. H2NO+NH2=HNO+NH3 3.00E+12 0.0 1000.0

108. H2NO+NO=HNO+HNO 2.00E+07 2.0 13000.0

109. H2NO+NO2=HONO+HNO 6.00E+11 0.0 2000.0

110. H2NO+O=HNO+OH 3.00E+07 2.0 2000.0

111. H2NO+O=NH2+O2 4.00E+13 0.0 0.0

112. HNNO+NO=N2+HONO 2.60E+11 0.0 1620.0

113. HNNO+NO=NNH+NO2 3.20E+12 0.0 540.0

114. HNOH+M=>H+HNO+M 1.03E+04 -4.8 59527.0

115. HO2+H=O+H2O 3.00E+13 0.0 1721.0

116. HONO+H=HNO+OH 5.64E+10 0.9 4969.0

117. HONO+H=NO+H2O 8.13E+06 1.9 3846.0

118. HONO+HONO=NO+NO2+H2O 9.69E+10 0.0 14132.0
119. HONO+NH=NH2+NO2 1.00E+13 0.0 0.0
120. N2H2+H=NNH+H2 5.00E+13 0.0 1000.0
121. N2H2+M=NNH+H+M 5.00E+16 0.0 50000.0
122. N2H2+NH=NNH+NH2 1.00E+13 0.0 1000.0
123. N2H2+NH2=NNH+NH3 1.00E+13 0.0 1000.0
124. N2H2+NO=N2O+NH2 3.00E+12 0.0 0.0
125. N2H2+O=NH2+NO 1.00E+13 0.0 1000.0
126. N2H2+O=NNH+OH 2.00E+13 0.0 1000.0
127. N2H2+OH=NNH+H2O 1.00E+13 0.0 1000.0
128. N2H3+H=NH2+NH2 1.60E+12 0.0 0.0
129. N2H3+M=N2H2+H+M 3.50E+16 0.0 46000.0
130. N2H3+NH=N2H2+NH2 2.00E+13 0.0 0.0
131. N2H3+O=N2H2+OH 5.00E+12 0.0 5000.0
132. N2H3+O=NH2+HNO 1.00E+13 0.0 0.0
133. N2H3+OH=N2H2+H2O 1.00E+13 0.0 1000.0
134. N2H3+OH=NH3+HNO 1.00E+12 0.0 15000.0
135. N2H4+H=N2H3+H2 1.30E+13 0.0 2500.0
136. N2H4+NH2=N2H3+NH3 3.90E+12 0.0 1500.0
137. N2H4+O=N2H2+H2O 8.50E+13 0.0 1200.0
138. N2H4+OH=N2H3+H2O 4.00E+13 0.0 0.0
139. NH2+HO2=H2NO+OH 2.50E+13 0.0 0.0
140. NH2+NH=N2H2+H 5.00E+13 0.0 0.0
141. NH2+NH2=N2H2+H2 8.50E+11 0.0 0.0
142. NH3+HNO3=H2NO+H2O+NO 2.32E+01 3.5 44926.0
143. NNH=N2+H 1.00E+06 0.0 0.0
144. H2NO+OH=HNO+H2O 2.00E+07 2.0 999.0

145. N2H2+OH=>H2O+N2+H	2.50E+12	0.0	0.0
146. NH2+OH+M=H2NOH+M	5.00E+17	0.0	0.0
147. NO3+H=NO2+OH	6.00E+13	0.0	0.0
148. NO3+HO2=NO2+O2+OH	1.50E+12	0.0	0.0
149. NO3+NO2=NO+NO2+O2	4.90E+10	0.0	2937.4
150. NO3+O=NO2+O2	1.00E+13	0.0	0.0
151. NO3+OH=NO2+HO2	1.00E+13	0.0	0.0

NOTE: A units mole-cm-sec-K, E units cal/mole

Appendix B

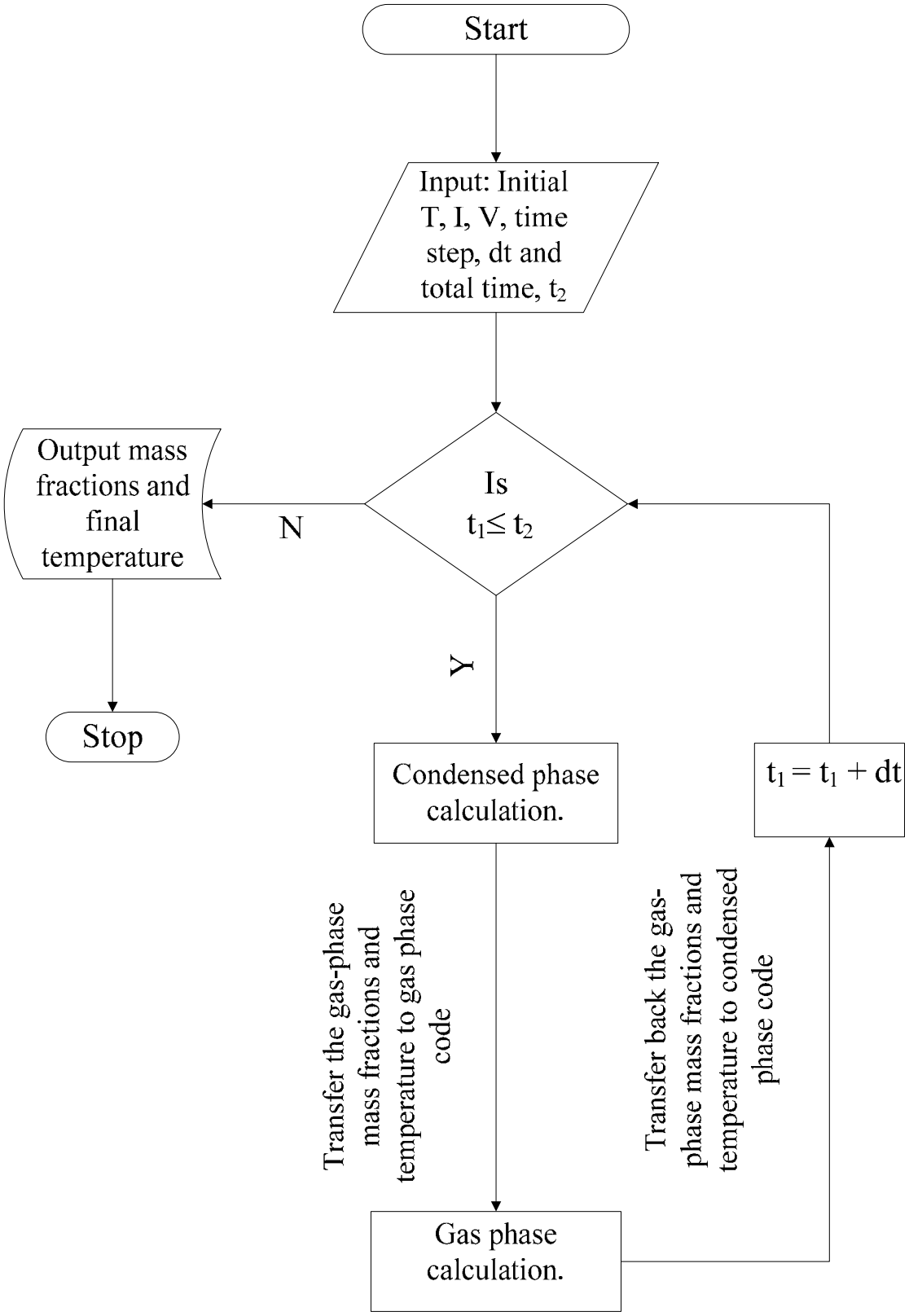
Start
Input: Initial T, I, V, time step, dt and total time, t_2
Is $t_1 \leq t_2$
N
Output mass fractions and final temperature
Stop
Y
Condensed phase calculation.
Transfer the gas-phase mass fractions and temperature to gas phase code
Gas phase calculation.
Transfer back the gas-phase mass fractions and temperature to condensed phase code
$t_1 = t_1 + dt$

Appendix C

Species considered and chemical mechanism used to simulate Propane ignition
Species Considered

1. C3H8	G	0	44.09721	298	3000	8	0	3	0
2. O2	G	0	31.99880	300	5000	0	2	0	0
3. N2	G	0	28.01340	300	5000	0	0	0	2
4. CO2	G	0	44.00995	300	5000	0	2	1	0
5. H2O	G	0	18.01534	300	5000	2	1	0	0
6. CO	G	0	28.01055	300	5000	0	1	1	0
7. H2	G	0	2.01594	300	5000	2	0	0	0
8. OH	G	0	17.00737	300	5000	1	1	0	0
9. O	G	0	15.99940	300	5000	0	1	0	0
10. H	G	0	1.00797	300	5000	1	0	0	0
11. HO2	G	0	33.00677	300	5000	1	2	0	0
12. H2O2	G	0	34.01474	300	5000	2	2	0	0
13. HCO	G	0	29.01852	300	5000	1	1	1	0
14. CH2O	G	0	30.02649	300	3000	2	1	1	0
15. CH3	G	0	15.03506	300	3000	3	0	1	0
16. CH2	G	0	14.02709	300	3000	2	0	1	0
17. CH	G	0	13.01912	300	3000	1	0	1	0
18. C2H4	G	0	28.05418	300	5000	4	0	2	0
19. C3H6	G	0	42.08127	298	3000	6	0	3	0
20. CH4	G	0	16.04303	300	3000	4	0	1	0
21. C2H6	G	0	30.07012	300	4000	6	0	2	0
22. C2H5	G	0	29.06215	298	3000	5	0	2	0
23. C2H3	G	0	27.04621	298	5000	3	0	2	0

24. C2H2 G 0 26.03824 300 5000 2 0 2 0

25. CH3CHO G 0 44.05358 298 3000 4 1 2 0

26. CH3CO G 0 43.04561 298 2000 3 1 2 0

27. CH2CO G 0 42.03764 300 5000 2 1 2 0

28. C3H7(N) G 0 43.08924 298 1500 7 0 3 0

29. C3H7(I) G 0 43.08924 298 1500 7 0 3 0

30. NO G 0 30.00610 300 5000 0 1 0 1

31. N G 0 14.00670 300 5000 0 0 0 1

Reactions Considered

(k = A T**b exp(-E/RT))

REACTIONS CONSIDERED	A	b	E
1. OH+H2=H2O+H	1.20E+09	1.3	3633.0
2. H+O2=O+OH	1.20E+17	-0.9	16520.0
3. H2+O=H+OH	1.80E+10	1.0	8900.0
4. H2O+O=OH+OH	1.60E+10	1.1	17304.0
5. H+H+M=H2+M	1.80E+18	-1.0	0.0
H2 Enhanced by 1.000E+00			
O2 Enhanced by 4.000E-01			
N2 Enhanced by 4.000E-01			
CO Enhanced by 7.500E-01			
CO2 Enhanced by 1.500E+00			
H2O Enhanced by 6.500E+00			
6. H+OH+M=H2O+M	2.20E+22	-2.0	0.0
H2 Enhanced by 1.000E+00			
O2 Enhanced by 4.000E-01			
N2 Enhanced by 4.000E-01			
CO Enhanced by 7.500E-01			
CO2 Enhanced by 1.500E+00			
H2O Enhanced by 6.500E+00			
7. H+HO2=OH+OH	1.50E+14	0.0	1004.0
8. H+HO2=H2+O2	2.50E+13	0.0	700.0
9. HO2+OH=H2O+O2	1.50E+13	0.0	0.0
10. HO2+O=O2+OH	2.00E+13	0.0	0.0

11. CO+OH=CO2+H 4.40E+06 1.5 -740.0

12. CH4+H=CH3+H2 2.20E+04 3.0 8750.0

13. CH4+O=CH3+OH 1.20E+07 2.1 7650.0

14. CH4+OH=CH3+H2O 1.50E+06 2.1 2460.0

15. CH3+O=CH2O+H 7.00E+13 0.0 0.0

16. CH2O+H=HCO+H2 2.50E+13 0.0 4110.0

17. CH2O+O=HCO+OH 3.00E+13 0.0 3390.0

18. CH2O+OH=HCO+H2O 8.00E+13 0.0 1500.0

19. HCO+O2=CO+HO2 1.20E+13 0.0 910.0

20. HCO+H=CO+H2 2.00E+14 0.0 0.0

21. HCO+M=H+CO+M 7.10E+14 0.0 16800.0

H2 Enhanced by 1.000E+00

O2 Enhanced by 4.000E-01

N2 Enhanced by 4.000E-01

CO Enhanced by 7.500E-01

CO2 Enhanced by 1.500E+00

H2O Enhanced by 6.500E+00

22. CH3+CH3=C2H5+H 8.00E+14 0.0 26500.0

23. CH3+CH3=C2H4+H2 1.00E+16 0.0 32000.0

24. C2H6+H=C2H5+H2 5.40E+02 3.5 5210.0

25. C2H6+O=C2H5+OH 3.00E+07 2.0 5110.0

26. C2H6+OH=C2H5+H2O 6.30E+06 2.0 645.0

27. C2H5+O2=C2H4+HO2 2.00E+12 0.0 4995.0

28. O+C2H5=CH3CHO+H 5.00E+13 0.0 0.0

29. C2H4+O=CH3+HCO 2.00E+13 0.0 2290.0

30. OH+C2H4=CH3+CH2O 4.00E+13 0.0 1510.0

31. H+CH3CHO=CH3CO+H2 4.00E+13 0.0 4210.0

32. O+CH3CHO=CH3CO+OH 5.00E+12 0.0 1800.0

33. OH+CH3CHO=CH3CO+H2O 1.00E+13 0.0 0.0

34. CH3CO+M=CH3+CO+M 1.00E+15 0.0 9420.0

35. H+C2H4=C2H3+H2 1.50E+14 0.0 10200.0

36. H+C2H3=C2H2+H2 8.00E+12 0.0 0.0

37. O+C2H3=CH2CO+H 1.00E+13 0.0 0.0

38. C2H2+O=CH2+CO 5.00E+13 0.0 3700.0

39. OH+C2H2=CH2CO+H 4.00E+05 2.0 -690.0

40. H+CH2CO=CH3+CO 1.10E+13 0.0 3390.0

41. O+CH2CO=HCO+HCO 1.00E+13 0.0 2410.0

42. OH+CH2CO=CH2O+HCO 2.80E+13 0.0 0.0

43. CH2+O=CO+H+H 8.00E+13 0.0 0.0

44. CH2+O2=CO2+H+H 4.00E+13 0.0 2200.0

45. CH2+H=CH+H2 1.50E+13 0.0 0.0

46. C2H5+CH3=C3H8 2.00E+13 0.0 0.0

47. H+C3H8=H2+C3H7(N) 1.30E+14 0.0 9700.0

48. H+C3H8=H2+C3H7(I) 1.00E+14 0.0 8360.0

49. O+C3H8=OH+C3H7(N) 3.00E+13 0.0 5760.0

50. O+C3H8=OH+C3H7(I) 2.60E+13 0.0 4440.0

51. OH+C3H8=H2O+C3H7(N) 3.70E+12 0.0 1650.0

52. OH+C3H8=H2O+C3H7(I) 2.80E+12 0.0 860.0

53. C3H7(N)=C2H4+CH3 3.00E+14 0.0 33030.0

54. C3H7(I)=C3H6+H 2.00E+14 0.0 38740.0

55. C3H7(N)=C3H6+H 1.00E+14 0.0 37330.0

56. O+C3H6=CH3+CH3CO 5.00E+12 0.0 600.0

57. OH+C3H6=CH3+CH3CHO 7.00E+12 0.0 0.0

58. CH+O=CO+H 4.00E+13 0.0 0.0

59. CH+O2=CO+OH 2.00E+13 0.0 0.0

60. C2H3+O2=HCO+CH2O 4.00E+12 0.0 -250.0

61. H2O2+OH=H2O+HO2 1.00E+13 0.0 1800.0

62. HO2+HO2=H2O2+O2 2.00E+12 0.0 0.0

63. H2O2+H=HO2+H2 1.70E+12 0.0 3750.0

64. H2O2+M=OH+OH+M 1.20E+17 0.0 45500.0

65. CH2O+HO2=HCO+H2O2 1.00E+09 0.0 0.0

66. C3H8+HO2=C3H7(N)+H2O2 5.00E+12 0.0 18000.0

67. C3H8+HO2=C3H7(I)+H2O2 5.00E+12 0.0 18000.0

68. C2H6+HO2=C2H5+H2O2 3.00E+11 0.0 11500.0

69. H+O2+M=HO2+M 2.00E+18 -0.8 0.0

H2O Enhanced by 6.500E+00

CO2 Enhanced by 1.500E+00

CO Enhanced by 7.500E-01

O2 Enhanced by 4.000E-01

N2 Enhanced by 4.000E-01

70. C2H3+M=C2H2+H+M 3.00E+15 0.0 32027.0

71. CH4=CH3+H 2.80E+27 -4.0 103856.0

72. C2H6=CH3+CH3 2.00E+28 -3.7 91298.0

73. C2H5=C2H4+H 9.90E+22 -3.1 42662.0

74. O+N2=NO+N 1.80E+14 0.0 76249.0

75. N+O2=NO+O 1.80E+10 1.0 9300.0

76. N+OH=NO+H 7.10E+13 0.0 894.0

NOTE: A units mole-cm-sec-K, E units cal/mole